# Reconstruction of Complete 12-Lead ECGs from Incomplete Digitized ECG Printouts

Mohammadsina Hassannia[1], Matthew A. Reyna[1], Gari D. Clifford[1,2], and Reza Sameni[1,2]
[1]Department of Biomedical Informatics, Emory University, Atlanta, GA, USA
[2]Department of Biomedical Engineering, Georgia Institute of Technology, Atlanta, GA, USA

## Abstract

*Standard 12-lead ECG printouts allocate only 2.5 s per lead, resulting in 75% of samples missing after digitization, which presents a significant barrier to programmatic analysis and machine learning pipelines that require complete recordings. We propose a training-free signal-processing framework to reconstruct full 10-second, 12-lead ECGs in three stages: (i) missing limb and augmented lead segments are recovered analytically via Einthoven's law; (ii) a robust weighted beat template from each lead's observed window is replicated across the full recording using R-peaks from Lead II; and (iii) R-peak realignment and null-space projection enforce inter-lead consistency. On PTB-XL, mean SNR reaches 11.6–16.4 dB, with the projection step contributing up to 3.6 dB for limb and augmented leads. R-peak and QRS onset errors are near the quantization floor, and QT errors are clinically negligible, confirming that incomplete digitized ECG archives can be completed to a quality suitable for downstream analysis.*

## 1. Introduction

The standard 12-lead ECG remains the most widely used tools for the screening cardiovascular diseases, diagnosis of arrhythmias, ischemia, and a broad spectrum of cardiac conditions [1, 2]. It provides a comprehensive spatial representation of cardiac electrical activity through a combination of limb leads (I, II, III), augmented leads (aVR, aVL, aVF), and precordial leads (V1–V6). Despite the widespread transition to digital ECG acquisition systems over recent decades, a large and historically valuable proportion of records remains available only as paper printouts or scanned images, especially in resource limited settings and within historical datasets accumulated through routine clinical practice. Recent open-source initiatives, including the George B. Moody PhysioNet Challenge 2024 and a subsequent 2025–2026 Kaggle competition, have enabled digitization of ECG time series from such images [3,4]. However, digitized ECGs have a fundamental limitation: Standard 12-lead ECG printouts, such as those generated by GE MAC series machines, display only 2.5 s per lead, with a single lead (e.g. Lead II) printed at full length as a rhythm reference. Consequently, even a perfectly digitized printout yields an incomplete recording, with 75% of the samples missing from eleven out of twelve leads. This is a significant challenge for programmatic ECG analysis and machine learning pipelines that require full-length synchronous recordings across all leads. ECG imputation methods that recover a missing lead from the remaining observed leads [5, 6] are fundamentally different from the challenge of reconstructing missing 7.5 s segments of each lead, which is the focus of the present study. In this work, we present a signal processing based framework for reconstructing complete 10 s, 12-lead ECG recordings from partially observed signals after digitization of standard ECG printouts. We leverage two key properties of the ECG: *(i)* the linear inter-lead dependencies defined by Einthoven's law and augmented lead definitions, which impose mathematical constraints between leads, and *(ii)* the quasi-periodicity of the ECG, which enables a beat template learned from a short observed window to be extended to the missing segments.

## 2. Method

### 2.1. Overview of ECG Lead Relationships

The standard 12-lead ECG includes six limb leads (I, II, III, aVR, aVL, aVF), which are not mutually independent. Only leads I and II are commonly recorded from the body; lead III is obtained from Einthoven's law; aVR, aVL, and aVF are linearly obtained from leads I, II, and III. The precordial leads (V1–V6), however, are linearly independent. Defining a vector of 12-lead measurements with $n$ samples as $\mathbf{X} = [\mathrm{I}, \mathrm{II}, \mathrm{III}, \mathrm{aVR}, \mathrm{aVL}, \mathrm{aVF}, \mathrm{V1}, \ldots, \mathrm{V6}] \in \mathbb{R}^{12\times n}$, the linear constraints on these six leads can be mathematically expressed as:

$$\mathbf{A}\,\mathbf{X} = 0, \tag{1}$$

where $\mathbf{A} \in \mathbb{R}^{4\times 12}$ is the constraint matrix:

$$\mathbf{A} = \left(\begin{array}{cccccc|c} 1 & -1 & 1 & 0 & 0 & 0 & \\ 1 & 1 & 0 & 2 & 0 & 0 & \\ 2 & -1 & 0 & 0 & -2 & 0 & 0_{4\times 6} \\ -1 & 2 & 0 & 0 & 0 & -2 & \end{array}\right), \tag{2}$$

We can show that $\mathrm{rank}(\mathbf{A}) = 4$, i.e., the constraints remove four degrees of freedom from the twelve leads, leav-

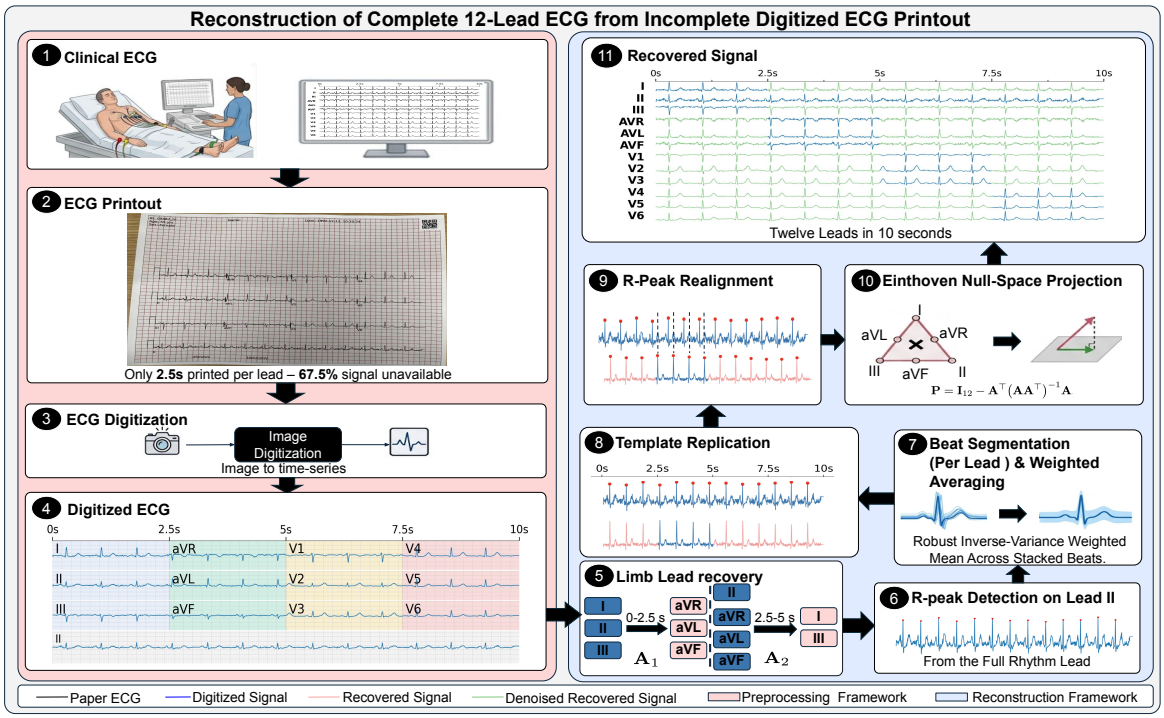


Figure 1: End-to-end reconstruction pipeline. *Preprocessing* (pink): a clinical ECG printout is digitized, yielding only 2.5 s per lead. *Reconstruction* (blue): missing limb lead windows are recovered via Einthoven constraints (Box 5); R-peaks from Lead II (Box 6) anchor per-lead beat templates (Box 7) replicated across 10 s (Box 8). R-peaks are re-detected on each reconstructed lead and used to calibrate Lead II reference timing for beat replication (Box 9). *Postprocessing* (Box 10): Null-space projection enforce inter-lead relationship consistency. Box 11: final 12-lead reconstruction.

ing an effective signal subspace of dimension $12 - 4 = 8$. Consequently, any standard 12-lead ECG must lie in the null space of $\mathbf{A}$, denoted $\ker(\mathbf{A})$, which forms an 8-dimensional subspace of $\mathbb{R}^{12}$. The orthogonal projector onto $\ker(\mathbf{A})$ is given by:

$$\mathbf{P} = \mathbf{I}_{12} - \mathbf{A}^\top \left(\mathbf{A}\mathbf{A}^\top\right)^{-1}\mathbf{A}, \tag{3}$$

which is idempotent, i.e., satisfies $\mathbf{P}^2 = \mathbf{P}$. This projector plays a central role in enforcing inter-lead mathematical relationship, as described in Section 2.2.3. In addition to enforcing inter-lead relationship, it can serve as a spatial ECG denoiser. Any component of the measurements lying outside $\ker(\mathbf{A})$, introduced by post-measurement noise or the digitization process, can be eliminated by the projection and only the physically acceptable signal subspace that satisfy the ECG lead inter-relationships is retained.

## 2.2. Proposed algorithm

We derive the proposed algorithm for printouts in the 4-by-2.5 s + one 10 s rhythm-lead format, which is the most common format used, for example, in GE MAC series ECG devices. A similar methodology, but with different matrix transformations, can be derived for other ECG formats. This format, visualizes the 12 lead ECG across four strips, each spanning 10 s. (Box 2 in Fig.1). Only a 2.5 s window is available for leads I, II and III over $[0,\ 2.5]$ s, aVR–aVF over $[2.5,\ 5]$ s, V1–V3 over $[5,\ 7.5]$ s, and V4–V6 over $[7.5,\ 10]$ s. One of the limb leads (often Lead II) is also available at full 10 s length as a rhythm reference in the last row, but temporally synchronous with the 2.5 s segments of the first three rows (Box 4 in Fig.1). Therefore, except for the rhythm lead, all other leads have 7.5 s of missing samples that we want to estimate using the inter-lead relationships. Our proposed pipeline consists of three stages, illustrated in Fig. 1. Stage 1 enforces the linear constraints between the limb leads and the augmented limb leads. Stage 2 uses the rhythm lead to detect R-peaks, derives beat templates from the available segments of the short leads, uses these templates to impute the missing segments, and realigns the R-peaks to fix small timing shifts between leads. Stage 3 performs postprocessing through Einthoven-constrained projection to enforce the mathematical relationships among the leads.

### 2.2.1. Limb lead & augmented lead recovery

The first 2.5 s segments of the images displays only leads I, II and III; the second 2.5 s shows lead II (from the rhythm strip) and aVR, aVL and aVF. Using (1), due to

the linear dependency of the limb leads and the augmented limb leads, the missing segments of the first 5 s can be retrieved as follows:

$$\begin{bmatrix} \text{aVR} \\ \text{aVL} \\ \text{aVF} \end{bmatrix} = \underbrace{\frac{1}{2}\begin{pmatrix} -1 & -1 & 0 \\ 1 & 0 & -1 \\ 0 & 1 & 1 \end{pmatrix}}_{\mathbf{A}_1} \begin{bmatrix} \text{I} \\ \text{II} \\ \text{III} \end{bmatrix}, \tag{4}$$

$$\begin{bmatrix} \text{I} \\ \text{III} \end{bmatrix} = \underbrace{\frac{1}{6}\begin{pmatrix} 3 & -2 & 4 & -2 \\ 3 & 2 & -4 & 2 \end{pmatrix}}_{\mathbf{A}_2} \begin{bmatrix} \text{II} \\ \text{aVR} \\ \text{aVL} \\ \text{aVF} \end{bmatrix}. \tag{5}$$

where both $\mathbf{A}_1$ and $\mathbf{A}_2$ are obtained from the constraints in (2). From (5), the second system is overdetermined (four known segments and two unknown). Therefore, applying $\mathbf{A}_2$ involves some spatial filtering as well. Applying (4) and (5) extends the available segment of the limb and augmented leads from 2.5 s to 5 s (Box 5 in Fig. 1).

### 2.2.2. Missing segment beat imputation

The rhythm lead is the only lead recorded over the entire 10 s and is time-aligned with all 2.5 s segments. We therefore use the rhythm lead to determine when each heartbeat occurs, including during intervals where the other leads are missing. For this, we apply an R-peak detector (the `peak_det_likelihood.m` function from OSET in our case [7]) to Lead II to obtain the R-peak locations $r_k$ over the full 10 s. These R-peaks provide a common beat-timing reference for all leads (Box 6 in Fig. 1). Due to the vectorial nature of the cardiac electrical activity, small lead-specific timing offsets exist between the R-peaks of Lead II and those of the other leads (within several milliseconds).

For each lead, we then use its available segment to estimate the morphology of a representative beat. Beat epochs are extracted around the Lead II R-peaks that fall within the observed segment of that lead. We set the epoch length to the longest RR interval in the observed segment so that each epoch contains a complete cardiac cycle. These epochs are combined into an average lead-specific beat template using the robust weighted averaging method of [8] (available in the OSET function `robust_weighted_average.m`). Beats that deviate more from the mean receive lower weights, reducing the influence of noisy or atypical beats (Box 7 in Fig. 1).

Finally, the lead-specific template is replicated at every Lead II R-peak location across the full 10 s recording in the missing segments of other leads. In this way, the observed segment of each lead determines the beat morphology for each lead, while Lead II determines where those beats are placed in the missing segments. When two adjacent template copies overlap, the reconstructed sample is computed as a weighted average of the overlapping values, with weights inversely proportional to the inter-beat variance at that position (Box 8 in Fig. 1).

Since all leads are imputed using the Lead II R-peaks, small systematic timing offsets can remain between leads. To correct, R-peaks are re-detected on each reconstructed lead and compared with Lead II reference over the observed window. The mean difference gives a per lead offset $\delta$, and the shifted locations $r_k + \delta$ are used to repeat the template replication of Section 2.2.2 (Box 9 in Fig. 1).

### 2.2.3. Postprocessing: null space projection

To this point of the algorithm, we have recovered all missing segments. We apply a final null-space projection as postprocessing. Let $\hat{\mathbf{X}} \in \mathbb{R}^{12\times n}$ denote the reconstructed 12-lead ECG after realignment, i.e., the estimate of the true signal $\mathbf{X}$ produced by Stages 1 and 2. Since each lead is imputed independently, the reconstruction error $\hat{\mathbf{X}} - \mathbf{X}$ does not perfectly fulfil the inter-lead constraint (1). Therefore, we re-applying the projector $\mathbf{P}$ from (3) to obtain the final reconstruction:

$$\tilde{\mathbf{X}} = \mathbf{P}\,\hat{\mathbf{X}}, \tag{6}$$

which is the closest signal to $\hat{\mathbf{X}}$ satisfying $\mathbf{A}\tilde{\mathbf{X}} = 0$. Due to the form of $\mathbf{A}$, this stage only impacts the limb and augmented-limb leads (Box 10 in Fig. 1).

## 3. Results

We used 21,837 12-lead 10 s records from the PTB-XL dataset [9], to evaluate our algorithm. The time segments matching the GE MAC machine printed ECG segments were used to recover the full 12-lead 10 s records. Signal-to-noise ratio (SNR) and accuracy of multi-lead fiducial point estimation using the ground-truth vs recovered signals were used as performance metrics.

*1) SNR on the missing segments:* Table 1 and Fig. 2 present the SNR on the reconstructed segments across all records. After the beat imputation stage (Section 2.2.2), the mean SNR ranges from 10.2 dB (aVL) to 14.1 dB (V5). The null space projection postprocessing (Section (2.2.3)) consistently improves the SNR in all limb and augmented limb leads, with increases up to 3.6 dB (aVF) and 3.6 dB (aVR), while the precordial leads V1–V6 remain unaffected as expected.

*2) Fiducial Point Accuracy:* Fiducial points were extracted using the OSET package [7], from the original 12-lead waveforms and the waveforms recovered by our algorithm. Table 1 reports fiducial errors between the final outputs and ground truth. R-peak errors were computed by detecting peaks independently on both signals; for $\mathrm{Q_{on}}$, $\mathrm{T_{off}}$, and QT the R-peaks from the ground-truth detections were used as reference to avoid compounding errors between R-peaks and other fiducial points. R-peak localization error was below 2.1 ms, which is close to quantization noise floor (one sample at 500 Hz). $\mathrm{Q_{on}}$ error was below

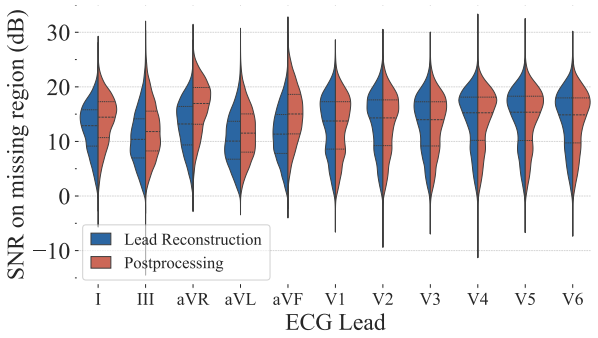


Figure 2: Per-lead SNR distribution on missing segments, after lead reconstruction and postprocessing stages.

Table 1: Lead recovery SNR and fiducial point errors (mean $\pm$ std) on recovered segments across all PTB-XL records.

| Lead | SNR (dB) | $\Delta$ R-peak (ms) | $\Delta Q_{on}$ (ms) | $\Delta T_{off}$ (ms) | $\Delta$ QT (ms) |
|---|---|---|---|---|---|
| I | $13.9 \pm 4.5$ | $1.27 \pm 4.75$ | $7.3 \pm 10.2$ | $11.8 \pm 16.6$ | $+7.45 \pm 20.71$ |
| III | $12.1 \pm 5.0$ | $1.98 \pm 4.81$ | $5.8 \pm 9.6$ | $21.0 \pm 26.7$ | $+10.25 \pm 32.21$ |
| aVR | $16.4 \pm 4.7$ | $0.92 \pm 3.34$ | $5.7 \pm 8.9$ | $9.0 \pm 13.0$ | $+5.40 \pm 17.75$ |
| aVL | $11.6 \pm 4.7$ | $2.09 \pm 5.26$ | $6.7 \pm 9.2$ | $20.0 \pm 25.5$ | $+10.20 \pm 32.20$ |
| aVF | $15.0 \pm 5.0$ | $1.68 \pm 4.86$ | $5.1 \pm 8.8$ | $11.6 \pm 19.1$ | $+5.62 \pm 22.41$ |
| V1 | $12.9 \pm 5.5$ | $1.48 \pm 4.01$ | $4.2 \pm 6.5$ | $23.2 \pm 29.5$ | $+10.47 \pm 35.85$ |
| V2 | $13.3 \pm 5.5$ | $1.84 \pm 4.99$ | $2.6 \pm 5.0$ | $11.8 \pm 24.0$ | $+3.33 \pm 25.60$ |
| V3 | $13.1 \pm 5.3$ | $1.96 \pm 5.43$ | $2.7 \pm 6.1$ | $8.9 \pm 18.7$ | $+3.08 \pm 20.72$ |
| V4 | $14.0 \pm 5.4$ | $1.53 \pm 4.51$ | $3.1 \pm 6.9$ | $9.8 \pm 18.2$ | $+3.85 \pm 19.84$ |
| V5 | $14.1 \pm 5.4$ | $1.28 \pm 4.24$ | $4.5 \pm 8.9$ | $10.7 \pm 18.9$ | $+4.73 \pm 21.81$ |
| V6 | $13.7 \pm 5.5$ | $1.30 \pm 4.77$ | $5.6 \pm 9.7$ | $12.1 \pm 20.7$ | $+6.00 \pm 24.16$ |

8 ms in all leads. The largest errors were in $T_{off}$, from 8.9 ms in V3 to 23.2 ms in V1, driving the corresponding QT errors spanning $3.1 - 10.5$ ms.

## 4. Discussion & Conclusion

The proposed method enables reconstructing 10 s, 12-lead ECG recordings from partial signals produced by digitizing standard paper printouts. Limb lead recovery using intrinsic ECG redundancy, and beat-template imputation recovers the missing segments with up to an SNR of 10–14 dB. The subsequent null space projection enforces the Einthoven law, further improving the SNR by around 3.5 dB in the limb and augmented leads, while leaving precordial leads V1–V6 unaffected. Fiducial point errors confirm clinical utility. R-peak errors are at the quantization noise floor ($\approx$ 2 ms at 500 Hz sampling frequency). $Q_{on}$ errors are below 8 ms across all leads; $T_{off}$ has a larger error of around 23 ms, which aligns the literature on the Cramér-Rao lower bounds for T-wave offset detection [10]. QT interval error is therefore largely driven by the T-wave offset error, but still in an acceptable clinical range [11].

The method relies on the internal relationship between ECG leads, making it applicable to any digitized ECG archive where complete recordings are unavailable. Future work should evaluate diagnostic performance on ECGs recovered by the proposed algorithm, applied to ECG waveforms digitized from real ECG images. The method can also be generalized to other forms of ECG printouts.

## References

[1] Huang J, Chen B, Yao B, He W. ECG Arrhythmia Classification Using STFT-Based Spectrogram and Convolutional Neural Network. IEEE Access 2019;7:92871–92880.

[2] Shah A, Singh D, Mohamed HG, Bharany S, Rehman AU, Hussen S. Electrocardiogram Analysis for Cardiac Arrhythmia Classification and Prediction Through Self-Attention Based Autoencoder. Scientific Reports 2025;15(1):9230.

[3] Reyna MA, Deepanshi, Weigle J, Koscova Z, Campbell K, Seyedi S, Elola A, Bahrami Rad A, Shah AJ, Bhatia NK, Clifford GD, Sameni R. Digitization and Classification of ECG Images: The George B. Moody PhysioNet Challenge 2024. In Computing in Cardiology (CinC), volume 51. IEEE, 2024; 1–4.

[4] Reyna MA, Deepanshi, Weigle J, Koscova Z, Campbell K, Seyedi S, Elola A, Bahrami Rad A, Shah AJ, Bhatia NK, Yan Y, Dane S, Howard A, Clifford GD, Sameni R. PhysioNet Challenge 2024: Digitization of ECG Images. https://kaggle.com/competitions/physionet-ecg-image-digitization, 2025. Kaggle competition.

[5] EPMoghaddam D, Banta A, Post A, Razavi M, Aazhang B. Reconstructing 12-Lead ECG from Reduced Lead Sets Using an Encoder–Decoder Convolutional Neural Network. Biomedical Signal Processing and Control 2025; 104:107486. ISSN 1746-8094.

[6] Mason F, Pandey AC, Gadaleta M, Topol EJ, Muse ED, Quer G. AI-Enhanced Reconstruction of the 12-Lead Electrocardiogram via 3 Leads with Accurate Clinical Assessment. npj Digital Medicine 2024;7:201.

[7] Sameni R. The Open-Source Electrophysiological Toolbox (OSET). https://github.com/alphanumericslab/OSET, 2006–2026. Version 4.

[8] Leski JM. Robust Weighted Averaging of Biomedical Signals. IEEE Transactions on Biomedical Engineering aug 2002;49(8):796–804.

[9] Wagner P, Strodthoff N, Bousseljot RD, Kreiseler D, Lunze FI, Samek W, Schaeffter T. PTB-XL, a large publicly available electrocardiography dataset. Scientific Data May 2020; 7(1). ISSN 2052-4463.

[10] Fattahi D, Sameni R. Cramér-Rao Lower Bounds of Model-Based Electrocardiogram Parameter Estimation. IEEE Transactions on Signal Processing 2022;70:3181–3192. ISSN 1941-0476.

[11] Li Q, Barnett K, Xue J, Albert DE, Deepanshi, Rad AB, Sameni R, Clifford GD. Fusion-based QT interval estimation for enhanced long QT detection on a South African population using mobile ECG. Physiological Measurement February 2026;47(2):025011. ISSN 1361-6579.

Address for correspondence:

Reza Sameni (rsameni@dbmi.emory.edu), Emory University School of Medicine, Atlanta, GA 30322 USA